PROCEEDINGS OF SCIENCE

Deciphering the Secrets of the Long-Lived Particles at the Colliders

Chandrima Sen,[a,*] **Priyotosh Bandyopadhyay,**[a] **Mariana Frank**[b] **and Snehashis Parashar**[a]

[a] *Indian Institute of Technology Hyderabad, Kandi, Sangareddy-502285, Telangana, India*
[b] *Department of Physics, Concordia University, 7141 Sherbrooke St. West, Montreal, Quebec, Canada H4B-1R6*
E-mail: ph19resch11014@iith.ac.in, bpriyo@phy.iith.ac.in, mariana.frank@concordia.ca, ph20resch11006@iith.ac.in

Conventional searches at the LHC operate under the assumption that Beyond the Standard Model particles undergo immediate decay upon production. However, this assumption lacks inherent a priori justification. In this study, we focus on displaced decay signatures, investigating their potential in both current and future collider experiments. Specifically, we examine the interactions between inert Higgs doublet (IDM) dark matter and a vector-like $SU(2)$ triplet lepton (VLL), both of which are Z_2-odd. While the vector current of the Z-boson with the VLL rules out a fermionic or two-component dark matter scenario, a compressed mass spectrum combined with a small Yukawa coupling permits co-annihilation and late decay of the VLL into the IDM sector, impacting the relic density of the pseudoscalar dark matter. These conditions also allow for displaced decays of the VLL, resulting in distinctive hadronically quiet, displaced multi-lepton signatures. Such signatures are analyzed in the context of the 14 and 27 TeV LHC, as well as the 100 TeV FCC-hh.

42nd International Conference on High Energy Physics (ICHEP2024)
18-24 July 2024
Prague, Czech Republic

[*] Speaker

PoS(ICHEP2024)280

1. Theoretical framework

The particle content of the SM is extended with an additional $SU(2)_L$ scalar doublet (Φ_2), and one generation of a vector-like $SU(2)_L$ triplet lepton (N), with a hypercharge of $Y = -1$, following the convention $Q = T_3 + Y$. Since N is vector-like, both its left- and right-chiral components, $N_{L,R}$, transform identically under $SU(2)_L$. Additionally, a discrete Z_2 symmetry is imposed on the particle content, making all SM particles even while the new particles, Φ_2 and N, are odd.

Due to its Z_2-odd nature, Φ_2 does not couple to SM fermions, while Φ_1 couples to both quarks and leptons. However, Φ_2 can couple to the Z_2-odd vector-like lepton through the dark Yukawa coupling $\mathcal{Y}_N$, as illustrated below, where M_N is the Dirac mass for the vector-like lepton.

$$\mathcal{L}_{VLL} \supset \left[-\frac{M_N}{2} \overline{N_L} N_R + \mathcal{Y}_N \overline{L_L^e} N_R \Phi_2 \right] + h.c. \tag{1}$$

Here, the mass term for the VLL is Dirac, and it is not feasible to write a gauge- and Lorentz-invariant Majorana mass term for a VLL. Hence, our model by itself does not generate neutrino mass via any Seesaw mechanism,

2. Dark Matter constraints

In this framework, two neutral Z_2-odd candidates are present: N^0 and A^0 from the fermionic and the scalar sector,respectively. Being a component of non-zero hypercharged triplet fermionic field, N^0 has a non-zero vector current coupling with the Z-boson, resulting in high dark matter-nucleon scattering cross-sections. Consequently, N^0 is definitively excluded as a dark matter candidate by direct detection experiments [1]. This exclusion also invalidates the multi-component scenario, leaving A^0 as the sole viable dark matter candidate because, due to the CP-conserving nature of the Lagrangian, A^0 does not couple to the Z boson. However, if we consider a compressed mass spectrum between the Z_2-odd particles along with small Yukawa couplings $\mathcal{Y}_N$, these conditions can facilitate significant interplay through co-annihilation and late decay effects, impacting the relic density of A^0.

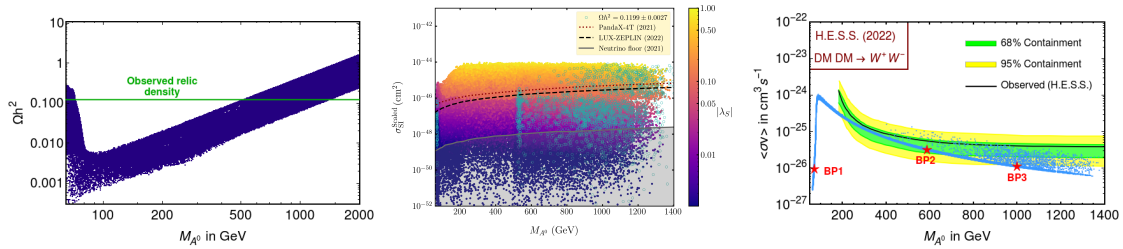

(a) (b) (c)

Figure 1: (a) DM mass (M_{A^0}) versus the DM relic density, (b) Scaled SI cross-section versus DM mass, with bounds from LZ, PandaX-4T experiments and (c) DM indirect detection bounds on the $\langle\sigma v\rangle$ of A^0 in the W^+W^- annihilation channel from H.E.S.S. experiment.

The interplay between the scalar dark sector (Φ_2) and the fermionic dark sector (N) results in a set of coupled Boltzmann equations. These equations can be solved using the `darkOmegaNTR` routine in `micrOMEGAs` 5.3.41 [2] to determine the yields of both sectors. Here, we have chosen the mass of the fermionic dark sector to be higher than that of the scalar dark sector. Hence, the charged and neutral fermionic states can decay into the scalar states, depending on the dark Yukawa couplings and the compressed mass spectrum.

After solving the appropriate coupled Boltzmann equations, including the decay effect, we obtain a plot of M_{A^0} versus the dark matter relic density Ωh^2, as shown in Figure 1 (a). The green band represents the observed relic density of $\Omega h^2 = 0.1199 \pm 0.0027$ [3]. We observe a lower mass region around 70 GeV that satisfies the relic density, which is attributed to the s-channel resonance through the SM Higgs boson. Masses above 1.4 TeV are ruled out being overabundant. Next we focus on the spin-independent (SI) DM-nucleon scattering cross-section $\sigma_{\rm SI}$ in Figure 1 (b). Considering the most stringent bound from the LUX-ZEPLIN (LZ) [4] experiment, we can exclude $|\lambda_S| \gtrsim 0.5$ values within the relic-satisfying region of $M_{A^0} \in [500, 1400]$ GeV. Finally, we verify the parameter regions that satisfies the indirect detection results from H.E.S.S. experiment as well [5]. The most dominant annihilation mode of A^0 is W^+W^-, and we present the $\langle\sigma v\rangle$ values for points allowed by direct detection experiments, scaled according to the percentage contribution of that particular annihilation mode in Figure 1 (c). We chose three benchmark points (BPs) satisfying all the relevant bounds and shown them with red stars.

3. Interplay between Two Dark Sectors

Driven by dark matter constraints and further supported by limits from $h \to \gamma\gamma$, electroweak precision data (EWPD), and collider bounds on VLL [6], we identify three key BPs, which are outlined in Table 1, where we present the masses and pertinent couplings of the additional scalars and fermions within the model.

BP	M_{A^0} (GeV)	M_{H^0} (GeV)	$M_{H^\pm}$ (GeV)	M_{N^0} (GeV)	M_{N^-} (GeV)	$M_{N^{--}}$ (GeV)	λ_3	λ_S	$\mathcal{Y}_N$	Ωh^2
BP1	71.57	117.16	84.76	98.25	98.61	99.28	0.07	0.002	4.2×10^{-9}	0.119
BP2	587.6	589.4	588.2	595.5	595.9	596.8	0.05	0.03	1.1×10^{-7}	0.121
BP3	1000.0	1010.5	1001.0	1010.6	1011.0	1011.9	0.02	-0.04	5.4×10^{-7}	0.121

Table 1: Benchmark points BP1, BP2, and BP3, with the masses of the dark sector particles, the relevant couplings, and DM relic density values.

Based on the mass difference between the scalar and fermionic dark sectors and the Yukawa coupling values, the yields of the two neutral dark components exhibit distinct behaviours. Figure 2 illustrates this interplay for the three selected benchmark points, showing the yields of the two dark sectors, Y_{Φ_2} (solid blue line) and Y_N (dashed orange line), as a function of $x = M_{\rm DM}/T$.

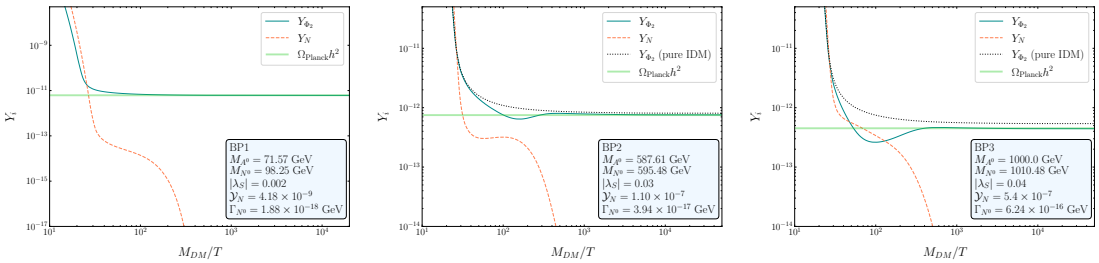

(a) (b) (c)

Figure 2: The DM yields Y_i as a function of $x = M_{\rm DM}/T$ for (a) BP1, (b) BP2, (c) BP3. The Y_{Φ_2} and Y_N are shown with blue solid line and orange dashed line respectively. For BP2 and BP3, the black dotted lines represent the yield for the same scalar masses for a pure IDM case, with no effect from the VLLs. The light green band represents the observed relic $\Omega_{\rm Planck}h^2 = 0.1199 \pm 0.0027$.

As illustrated in Figure 2(a), for BP1, the decay effects of N is almost negligible, resulting in A^0 decoupling with a higher yield than N. Although N remains in equilibrium slightly longer due to its relatively larger annihilation cross-section at lower mass before decoupling, it eventually decays later with a decay width of $\Gamma_N \sim 1.9 \times 10^{-18}$ GeV. In the case of BP2, N now decouples with a higher yield compared to BP1 due to its larger mass and decays with a width of $\Gamma_N \sim 3.9 \times 10^{-17}$ GeV. The yield of A^0 experiences a dip due to enhanced co-annihilation resulting from the compressed spectrum, which later receives contributions from the decay of N. For BP3, with both N and Φ_2 having mass scales around $O(1)$ TeV, N decouples earlier compared to the other BPs due to a reduction in its annihilation cross-section, with a decay width of $\Gamma_N \sim 6.2 \times 10^{-16}$ GeV.

For BP2 and BP3, we also show the yields for a pure IDM case (black dotted lines), where the fermionic sector does not affect the scalar/pseudoscalar DM evolution. Without the co-annihilation and decay of the VLL, a pure inert doublet DM shows overabundance for these two BPs. However, including the fermionic dark sector allows the scalar parameter points to fall within the region permitted by Planck data. Thus, the late decay of N becomes more significant for achieving the observed relic density, particularly at higher DM masses ($O \sim 1$ TeV).

It is significant now to examine the interplay between the pseudoscalar DM candidate A^0 and fermionic DM species N^0, particularly in the higher mass regions for BP2 and BP3. By fixing the masses of the inert scalars and the Higgs portal coupling, we varied the mass gap ($M_{N^0} - M_{A^0}$) from 1 to 200 GeV, while also scanning over a range of Yukawa couplings $\mathcal{Y}_N$ from 10^{-9} to 10^{-4}. We then tracked the relic density Ωh^2 for each point. The ratios of these relic densities to the central value of the Planck 2018 data on observed relic density, i.e. $\Omega_{\rm Planck} h^2 = 0.1199$, are presented in two-dimensional heatmap plots shown in Figure 3.

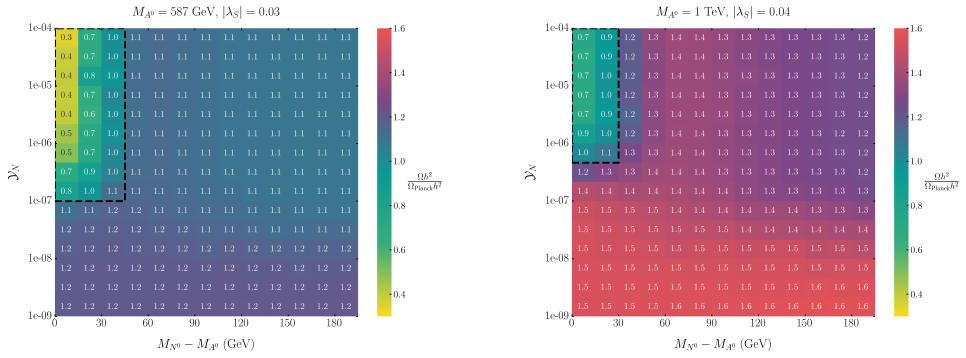

(a) (b)

Figure 3: Heatmap of pseudoscalar DM relic ratios $\frac{\Omega h^2}{\Omega_{\rm Planck} h^2}$, as a function of the mass gap $M_{N^0} - M_{A^0}$, and the Yukawa coupling $\mathcal{Y}_N$, fixing the scalar sector mass values in (a) BP2, (b) BP3.

In Figure 3(a), we display the relic ratios $\frac{\Omega h^2}{\Omega_{\rm Planck} h^2}$ for a pseudoscalar DM mass of 587 GeV, illustrating variations in the mass gap $M_{N^0} - M_{A^0}$ (in GeV) and the Yukawa coupling $\mathcal{Y}_N$. Each bin in the plot shows the mean relic ratios for the points scanned within that bin. A relic ratio of 1.0 indicates the correct relic abundance $\Omega_{\rm Planck} h^2 = 0.1199 \pm 0.0027$, while ratios below 1.0 indicate underabundance. Bins with $\frac{\Omega h^2}{\Omega_{\rm Planck} h^2} \geq 1.1$ are overabundant and are excluded by Planck data [3]. From Figure 3(a), the points that meet the relic density or show underabundance for the pseudoscalar DM mass of 587 GeV fall within a mass gap range of $(M_{N^0} - M_{A^0}) \in [1 - 45]$ GeV and a Yukawa coupling range of $\mathcal{Y}_N \in [10^{-7}, 10^{-4}]$. This viable region is highlighted with a black rectangle with thick dashed borders on the heat-map. In Figure 3(b), we present the same analysis for a pseudoscalar DM mass of 1 TeV, corresponding to BP3. The viable region for correct relic or underabundance, enclosed in a black dashed rectangle, is significantly smaller compared to BP2. For this higher mass scenario, the allowed parameter range narrows to $(M_{N^0} - M_{A^0}) \in [1 - 30]$

GeV and $\mathcal{Y}_N \in [5 \times 10^{-7}, 10^{-4}]$; beyond these ranges, overabundance occurs. In both plots, we see that overabundance saturates when the mass gap exceeds 100 GeV for $\mathcal{Y}_N \gtrsim 5 \times 10^{-8}$ bins, corresponding to the pure IDM yields discussed in Figure 2. The highest overabundance is observed when $\mathcal{Y}_N \lesssim 10^{-8}$, regardless of the mass gap. This is because such small Yukawa couplings do not significantly affect co-annihilation but lead to very late out-of-equilibrium decay of the fermions, increasing the number density of A^0.

This compressed spectrum and delayed decay effect influence the collider phenomenology of our model, leading to unique and interesting signatures of displaced vertices. In the next section, we will discuss the phenomenology of our model at the LHC and FCC-hh.

4. Collider Simulation at the LHC/FCC-hh

In this section, our focus is on investigating the production of the doubly-charged fermions ($N^{\pm\pm}$), and their displaced decays at the LHC/FCC-hh. The compressed mass spectra of the dark sector and the small Yukawa coupling values ensure the presence of displaced leptons for the benchmark points, which can be leveraged to identify novel signatures of exotic new physics.

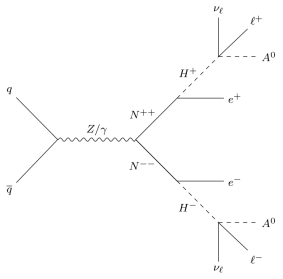

Figure 4: The pair production of $N^{\pm\pm}$ fields and its corresponding decays.

Figure 4 illustrates the relevant Feynman diagram for the pair production of $N^{\pm\pm}$ and its subsequent decay chains. The decay width for this process can be given as,

$$\Gamma_{N^{\pm\pm}\to H^\pm \ell^\pm} = \frac{\mathcal{Y}_N^2 M_{N^{\pm\pm}}}{32\pi}\left(1 - \frac{M_{H^\pm}^2}{M_{N^{\pm\pm}}^2}\right)^2. \tag{2}$$

It is clear from Equation 2 that, due to the compressed mass spectra and small Yukawa couplings, the decay width can be small and that leads to the displaced vertex signatures at the collider. The rest mass decay length of the particle in the laboratory frame can be enhanced at the high-energy colliders due to the receiving of the significant boost.

Figure 5 depicts the distribution of decay lengths for $N^{\pm\pm}$ produced via the mode $p\,p \to N^{++}N^{--}$ at three centre-of-mass energies: 14, 27, and 100 TeV, for the three BPs. For BP1, the lower mass values enable a significant boost effect, as illustrated in Figure 5(a). Here, the decay lengths of $N^{\pm\pm}$ can extend up to around 10 km, 30 km, and 100 km at the 14 TeV (red), 27 TeV (dark orange), and 100 TeV (blue) colliders, respectively. In contrast, BP2 and BP3 exhibit considerably shorter decay lengths due to their higher masses, which limit the boost effect, and larger $\mathcal{Y}_N$ values, which reduce their rest mass decay lengths as well. For BP2, the maximum achievable decay lengths are approximately 60 m, 150 m, and 700 m at the three centre-of-mass energies of 14, 27, and 100 TeV, respectively. The heavier $\sim$ 1 TeV mass of $N^{\pm\pm}$ in BP3 further suppresses the boost effect, resulting in maximum decay lengths of nearly 90 cm, 110 cm, and 1500 cm at colliders with 14, 27, and 100 TeV centre-of-mass energies, respectively.

As can be seen from Figure 4, this production mode is mediated by Z/γ interactions, and from this we can expect up to four displaced leptons. While displaced jets are also possible, their likelihood of being clustered is quite low, primarily due to the low momenta of the hadronic decay products from the off-shell

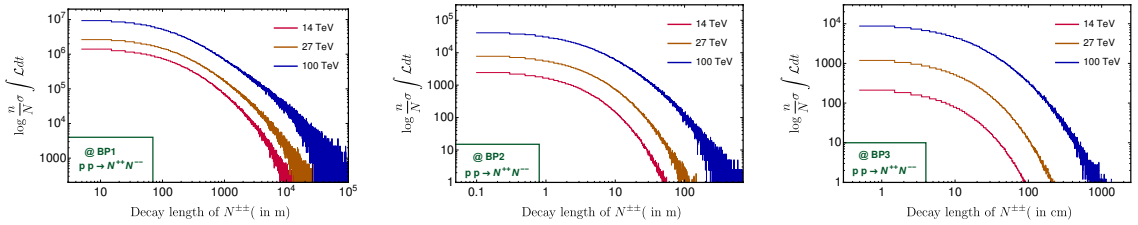

(a) (b) (c)

Figure 5: Displaced decay length distribution of N^{++}, coming from the pair production at the LHC/FCC-hh with the centre-of-mass energies of 14, 27 and 100 TeV for (a) BP1, (b) BP2, and (c) BP3. The number of events are normalized with the respective cross-sections and luminosity of 3000 fb^{-1}.

W-boson. The leptons, although anticipated to be soft because of the compressed spectrum, offer cleaner signatures than jets in the complex hadronic environment of the LHC/FCC-hh.

5. Discussion and conclusion

This study examines an extended Standard Model with a Z_2-odd inert Higgs doublet and a $Y = -1$ vector-like lepton triplet, focusing on their impact on dark matter relic abundance. The neutral VLL, due to its non-zero hypercharge and strong Z-boson coupling, cannot be the cold dark matter candidate. However, the VLL influences the relic abundance of pseudoscalar dark matter A^0 via late decay and co-annihilation, leading to specific predictions for the Yukawa coupling $\mathcal{Y}_N$ and mass splitting. With Yukawa couplings ranging from 10^{-9} to 10^{-7} and a mass spectrum between $O(100)$ GeV and $O(1)$ TeV, the doubly charged component ($N^{\pm\pm}$) of VLL can have displaced decay over the ranges from $O(10)$ cm to $O(1)$ km, producing up to four displaced leptons detectable by CMS, ATLAS, and MATHUSLA detectors.

6. Acknowledgement

CS would like to thank the MoE, Government of India for supporting her research via SRF. PB wants to thank SERB's MTR/2020/000668 grant for support during project. The work of MF has been partly supported by NSERC through the grant number SAP105354. SP acknowledges CSIR, India for funding his research.

References

[1] R. Essig, *Direct Detection of Non-Chiral Dark Matter*, *Phys. Rev. D* **78** (2008) 015004, [0710.1668].

[2] G. Alguero, G. Belanger, S. Kraml and A. Pukhov, *Co-scattering in micrOMEGAs: A case study for the singlet-triplet dark matter model*, *SciPost Phys.* **13** (2022) 124, [2207.10536].

[3] Planck collaboration, N. Aghanim et al., *Planck 2018 results. VI. Cosmological parameters*, *Astron. Astrophys.* **641** (2020) A6, [1807.06209]. [Erratum: Astron.Astrophys. 652, C4 (2021)].

[4] LZ collaboration, J. Aalbers et al., *First Dark Matter Search Results from the LUX-ZEPLIN (LZ) Experiment*, *Phys. Rev. Lett.* **131** (2023) 041002, [2207.03764].

[5] H.E.S.S. collaboration, H. Abdalla et al., *Search for Dark Matter Annihilation Signals in the H.E.S.S. Inner Galaxy Survey*, *Phys. Rev. Lett.* **129** (2022) 111101, [2207.10471].

[6] L3 collaboration, P. Achard et al., *Search for heavy neutral and charged leptons in e^+e^- annihilation at LEP*, *Phys. Lett. B* **517** (2001) 75–85, [hep-ex/0107015].